GNA14 Somatic Mutation Causes Congenital and Sporadic Vascular Tumors by MAPK Activation

Young H. Lim,[1,2,3] Antonella Bacchiocchi,[1] Jingyao Qiu,[3] Robert Straub,[1] Anna Bruckner,[4] Lionel Bercovitch,[5] Deepak Narayan,[6] Yale Center for Mendelian Genomics, Jennifer McNiff,[1,2] Christine Ko,[1,2] Leslie Robinson-Bostom,[5] Richard Antaya,[1,7] Ruth Halaban,[1] and Keith A. Choate[1,2,3,*]

Vascular tumors are among the most common neoplasms in infants and children; 5%–10% of newborns present with or develop lesions within the first 3 months of life. Most are benign infantile hemangiomas that typically regress by 5 years of age; other vascular tumors include congenital tufted angiomas (TAs), kaposiform hemangioendotheliomas (KHEs), and childhood lobular capillary hemangiomas (LCHs). Some of these lesions can become locally invasive and unresponsive to pharmacologic intervention, leading to significant complications. Recent investigation has revealed that activating mutations in *HRAS*, *KRAS*, *NRAS*, *GNAQ*, and *GNA11* can cause certain types of rare childhood vascular tumors, and we have now identified causal recurrent somatic activating mutations in *GNA14* by whole-exome and targeted sequencing. We found somatic activating *GNA14* c.614A>T (p.Gln205Leu) mutations in one KHE, one TA, and one LCH and a *GNA11* c.547C>T (p.Arg183Cys) mutation in two LCH lesions. We examined mutation pathobiology via expression of mutant *GNA14* or *GNA11* in primary human endothelial cells and melanocytes. *GNA14* and *GNA11* mutations induced changes in cellular morphology and rendered cells growth-factor independent by upregulating the MAPK pathway. Our findings identify *GNA14* mutations as a cause of childhood vascular tumors, offer insight into mechanisms of oncogenic transformation by mutations affecting Gaq family members, and identify potential targets for therapeutic intervention.

Childhood vascular tumors are a heterogeneous group of lesions. Most are benign infantile hemangiomas (IHs [MIM: 602089]); other entities include congenital tufted angiomas (TAs [MIM: 607859]), kaposiform hemangioendotheliomas (KHEs [MIM: 141000]), and childhood lobular capillary hemangiomas (LCHs [MIM: 140850]), also known as pyogenic granulomas.[1] Congenital hemangiomas are divided into rapidly involuting (RICH [MIM: 602089]) and non-involuting (NICH [MIM: 602089]) subtypes and, along with TAs, LCHs, and KHEs, are distinguished from IHs by their lack of glucose transporter 1 (GLUT-1) immunoreactivity.[1,2] These lesions can rarely be associated with Kasabach-Merritt syndrome (MIM: 141000), a potentially fatal complication characterized by consumptive thrombocytopenia and coagulopathy.[3] Diagnosis of vascular tumors remains challenging given the histological overlap, and although beta-blockers and steroids are efficacious for a large number of lesions, serious side effects including hypotension, hypoglycemia, and bradycardia can be encountered.[4–7] Surgery remains the most effective intervention for refractory lesions.

Postzygotic somatic mutations have been found in specific classes of vascular tumors: activating mutations in *HRAS* (HRas proto-oncogene, GTPase [MIM: 190020]), *KRAS* (KRAS proto-oncogene, GTPase [MIM:190070]), and *NRAS* (neuroblastoma RAS viral oncogene homolog [MIM: 164790]) and downstream effectors, including *BRAF* (B-Raf proto-oncogene, serine/threonine kinase [MIM: 164757]), are found in NICHs and in up to 10% of sporadic LCHs.[8,9] Recently, we and others discovered that activating mutations in *GNA11* (G protein subunit alpha 11 [MIM: 600998]) and *GNAQ* (G protein subunit alpha q [MIM: 139313]) are present in RICHs, NICHs, and placental chorangiocarcinomas.[10,11] Other vascular lesions, including port-wine stains (PWSs [MIM: 163000]) and Sturge-Weber syndrome (SWS [MIM: 185300]), harbor *GNAQ* mutations, and changes in residue Arg183 are consistently present in lesions from individuals with SWS.[12,13] Activated GNA11 and GNAQ mediate VEGFR2 phosphorylation in human umbilical vein endothelial cells (HUVECs), inducing cell proliferation.[14,15] *GNA11* and *GNAQ* mutations leading to p.Gln209Pro (c.626A>C) and p.Arg183Cys (c.547C>T) changes are also detected in nearly 50% of primary uveal melanomas, in 83% of blue nevi, and in affected tissues of the mosaic disorder phakomatosis pigmentovascularis, which features capillary malformations, dermal melanocytosis, nevus spilus, and nevus of Ota.[16,17]

We studied a cohort of congenital vascular tumors without evidence of GLUT-1 immunoreactivity, which included four TAs and three KHEs. TAs and KHEs share clinical and histological features and are considered to be part of the same neoplastic spectrum.[18] In addition, we examined 21 sporadic LCHs arising in childhood. The study protocol was approved by the Yale Human Investigation Committee, and subjects' written consent was obtained prior to participation. Genomic DNA was isolated from

[1]Department of Dermatology, School of Medicine, Yale University, New Haven, CT 06510, USA; [2]Department of Pathology, School of Medicine, Yale University, New Haven, CT 06510, USA; [3]Department of Genetics, School of Medicine, Yale University, New Haven, CT 06510, USA; [4]Departments of Dermatology and Pediatrics, School of Medicine, University of Colorado, Aurora, CO 80045, USA; [5]Department of Dermatology, Warren Alpert Medical School, Brown University, Providence, RI 02903, USA; [6]Section of Plastic Surgery, Department of Surgery, School of Medicine, Yale University, New Haven, CT 06510, USA; [7]Department of Pediatrics, School of Medicine, Yale University, New Haven, CT 06510, USA
*Correspondence: keith.choate@yale.edu
http://dx.doi.org/10.1016/j.ajhg.2016.06.010.

Table 1. Somatic *GNA14* and *GNA11* Mutations Cause Vascular Tumors

Sample	Age (Years)	Sex	Site	Diagnosis	Somatic Mutation	No. of Reads in Tissue		No. of Reads in Blood		p Value
						Ref.	Non-ref.	Ref.	Non-ref.	
V101	0	male	neck	KHE	*GNA14* c.614A>T (p.Gln205Leu)	81	8	96	0	2.4×10^{-3}
V102	0	male	abdomen	TA	*GNA14* c.614A>T (p.Gln205Leu)	NA[a]	NA[a]	NA[a]	NA[a]	NA
V103	2	male	cheek	LCH	*GNA14* c.614A>T (p.Gln205Leu)	NA[a]	NA[a]	NA[a]	NA[a]	NA
V104	12	male	scalp	LCH	*GNA11* c.547C>T (p.Arg183Cys)	55	16	NA[b]	NA[b]	NA
V105	2	male	cheek	LCH	*GNA11* c.547C>T (p.Arg183Cys)	NA[a]	NA[a]	NA[a]	NA[a]	NA

Abbreviations are as follows: KHE, kaposiform hemangioendothelioma; LCH, lobular capillary hemangioma; NA, not applicable; non-ref., non-reference; ref., reference; and TA, tufted angioma.
[a]Mutation identified by Sanger sequencing.
[b]Exome sequencing performed on tumor only.

lesions or unaffected epidermis via laser capture microdissection and then extracted with the DNeasy Blood & Tissue Kit (QIAGEN). DNA from blood or saliva was obtained via a standard phenol-chloroform protocol. All lesions were screened via Sanger sequencing for mutations across all exons of *HRAS*, *KRAS*, *NRAS*, *BRAF*, *GNAQ*, and *GNA11*.

An identical somatic *GNA11* mutation, c.547C>T (p. Arg183Cys) (GenBank: NM_002067.4), was found in two LCHs (2/21 [10%]; subjects V104 and V105; Table 1 and Figure S1). This mutation has not been previously identified in vascular tumors, although somatic mutation c.548G>A (p.Arg183Gln) in paralog *GNAQ* is common in capillary malformations and PWSs and has been found in a single case of secondary LCH arising within a PWS.[8,12,19] A recent survey of 16 congenital hemangiomas identified 12/16 (75%) lesions with *GNA11* and *GNAQ* mutations, but all were Pro or Leu substitutions at Gln209.[10]

We further analyzed subjects without a detected mutation. In these subjects, we employed whole-exome sequencing (WES), performed by the Yale Center for Genome Analysis, by using barcoded libraries from sheared genomic DNA (Table S1). We pooled tumor DNA to run four barcoded samples per lane and pooled blood samples to run six barcoded samples per lane and ran all on the Illumina HiSeq 2000 with 75 bp paired-end reads. Using the Burrows-Wheeler Aligner (BWA-MEM), we aligned reads to the hg19 human reference sequence (UCSC Genome Browser) and trimmed them to targeted intervals with Picard.[20,21] We employed a Perl script to remove PCR duplicates, recalibrated the resulting BAM files according to the Genome Analysis Toolkit (GATK) Best Practices, and called blood and tissue variants with the GATK Haplotype Caller.[21] We used MuTect to identify all single-nucleotide variants (SNVs), deletions, and insertions and used ANNOVAR to annotate all variants for functional impact.[22,23] Data were filtered for damaging mutations (missense and nonsense mutations, splice sites, and indels) that (1) had at least three non-reference reads in tissue and zero, one, or two non-reference reads in blood and (2) were absent in 1000 Genomes (May 2011 release), the National Heart, Lung, and Blood Institute (NHLBI) Exome Sequencing Project (ESP) Exome Variant Server (release ESP6500), and the Exome Aggregation Consortium (ExAC) Browser control set of >134,000 exomes (v.0.3). We used a one-tailed Fisher's exact test to compare blood and tissue read numbers and excluded variants with a p value greater than 1.0×10^{-2} (Table S2). We examined the remaining mutations with the Broad Institute Integrative Genomics Viewer (IGV) to screen for variants resulting from alignment error.[24]

Our first subject, V101, was a male infant who had a diffuse right supraclavicular mass complicated by Kasabach-Merritt syndrome, which was identified as a KHE by histologic examination (Figure 1).[25] WES identified in *GNA14* (G protein subunit alpha 14 [MIM: 604397]) a single heterozygous somatic SNV, c.614A>T (p.Gln205Leu), which was confirmed by Sanger sequencing (Table 1 and Figure S2). There was no evidence of copy-number variation, loss of heterozygosity, or secondary mutation (Figure S2). Subsequent Sanger sequencing of all seven exons of *GNA14* in the remaining two KHEs, four TAs, and 19 LCHs without mutations in *HRAS*, *KRAS*, *NRAS*, *BRAF*, *GNAQ*, or *GNA11* identified the same heterozygous *GNA14* c.614A>T (p.Gln205Leu) somatic mutation (GenBank: NM_004297.3) in one TA (V102; Figure 1, Table 1, and Figure S2) and one sporadic LCH (V103; Figure 1, Table 1, and Figure S2). V102 was a male infant who presented at 5 weeks of age with a 5.5 × 3.5 cm, firm, reddish-blue abdominal lesion with prominent draining vessels. Doppler ultrasound revealed fast-flow and high-resistance vascular signals, and a punch biopsy diagnosed the lesion as a TA. By 26 months of age, the lesion had markedly regressed and appeared as a slightly depressed, atrophic telangiectatic patch. V103 was an archival specimen of a sporadic LCH from the cheek of a 2-year-old boy. Our discovery of three independent lesions with a recurrent

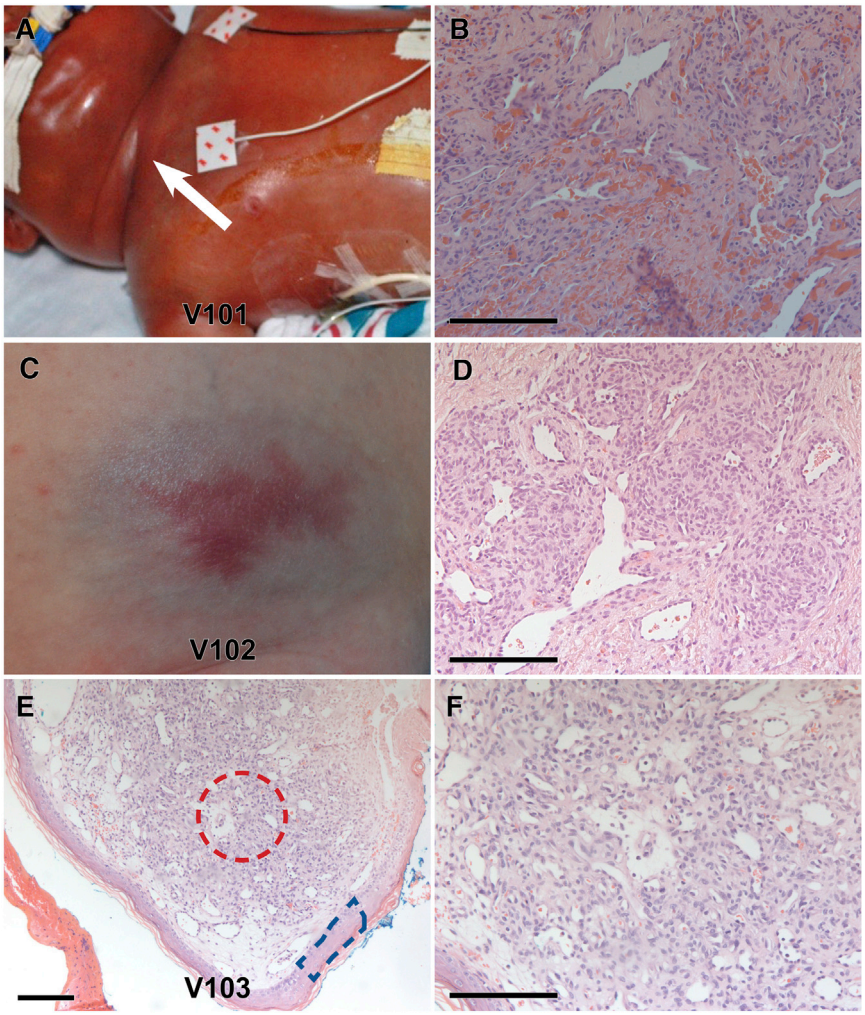

Figure 1. Somatic Activating Mutations in *GNA14* Cause Congenital and Sporadic Vascular Tumors

(A–D) Subjects V101 (A and B) and V102 (C and D) presented with a KHE (A, white arrow) and a TA, respectively. (B and D) Histology at 20× magnification demonstrates infiltrating nodules of spindled endothelial cells and intervening fibrous bands.

(E and F) 10× (E) and 20× (F) histology of V103, a sporadic lobular capillary hemangioma from the cheek of a 2-year-old male, demonstrates encapsulated lobules of proliferating vessels.

For samples where blood was unavailable (V102 and V103), sequencing was compared between laser capture microdissection of unaffected epidermis (E, blue box) and tumor (E, red circle). Scale bars represent 150 μm.

GNA14 mutation identifies GNA14 as a driver of childhood vascular tumors (Table 1).

GNA14, *GNA11*, and *GNAQ* encode G_α subunits that form a heterotrimer with G_β and G_γ subunits and bind to the cytosolic side of inactive seven-transmembrane G-protein-coupled receptors (GPCRs).[26,27] GPCRs bind a diverse array of ligands that activate the receptor, promoting the exchange of bound GDP to GTP on the G_α subunit. This facilitates the release of the G protein heterotrimer from the GPCR, as well as the dissociation of the activated G_α subunit from the β/γ dimer, leading to downstream activation of phospholipases, calcium channels, and other cellular pathways, including AKT and MAPK.[26,27]

Given that α subunit hydrolysis of GTP initiates the signaling cascade upon interaction with the GPCR, the properties of the α subunit define the functional characteristics of G proteins.[28] The G_α subunits are divided into four main families according to sequence homology: $G_{\alpha s}$, $G_{\alpha q}$, $G_{\alpha i}$, and $G_{\alpha 12}$ and $G_{\alpha 13}$.[29] Multiple members are within each family, and GNA14, GNA11, GNAQ, GNA15, and GNA16 belong to the $G_{\alpha q}$ family. Protein alignment of GNA14 to GNA11 and GNAQ shows close conservation, such that GNA14 Gln205 aligns with Gln209 of GNA11 and GNAQ and GNA14 Arg179 aligns with Arg183 of GNA11 and GNAQ, suggesting that mutations affecting GNA14 Arg179 could also cause vascular tumors (Figure S3). Of the 78 *GNA14* mutations listed in the Catalogue of Somatic Mutations in Cancer (COSMIC), one (c.536G>A [p.Arg179Gln]) was reported in malignant melanoma.[30]

To assess the molecular consequence of *GNA14* and *GNA11* mutations, we used Phyre2[31] to perform structural modeling for GNA14 and GNA11 and visualized them in Chimera[32] (Figure S4). Using an established structure of GNAQ as a template,[33] we inferred the structure of the GNA14 and GNA11 GTPase domain, which shares 92% homology with that of GNAQ (BLASTp). This revealed that all mutated residues fall at positions necessary for stabilizing the interaction between the GTPase catalytic domain and GTP. The GNAQ amide group of Arg183, which corresponds to Arg179 of GNA14 and Arg183 of GNA11, stabilizes the leaving γ-phosphate to facilitate hydrolysis.[34] GNAQ Gln209, corresponding to Gln205 of GNA14 and Gln209 of GNA11, lies in the switch II region and coordinates the critical nucleophilic water moiety responsible for hydrolysis of the γ-phosphate.[28,34] Compared to their native states, GNA14 p.Arg179Cys and GNA11 p.Arg183Cys increase the molecular distance of the side chains from the γ-phosphate by 3.766 and 3.002 Å, respectively, whereas GNA14 p.Gln205Leu and GNA11 p.Gln209Pro are moved away from the water molecule by 5.016 and 2.862 Å, respectively, destabilizing hydrolysis (Figure S4). Both substitutions are thus expected to generate a constitutively active GTP-bound subunit.[28,34]

To examine the pathobiology of the *GNA14* and *GNA11* mutations causing vascular tumors, we performed lentiviral

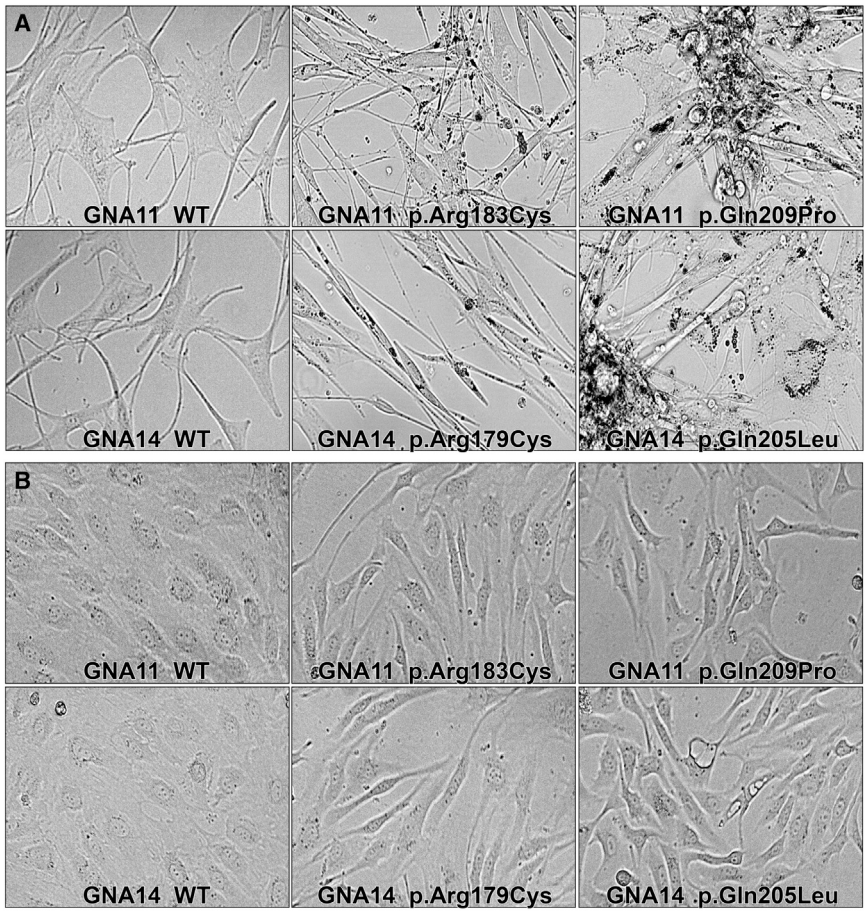

Figure 2. NBMELs and HUVECs Expressing Mutant *GNA14* and *GNA11* Demonstrate Morphological Changes

(A) 40× magnification of NBMELs with GNA11 p.Arg183Cys or GNA14 p.Arg179Cys and GNA11 p.Gln209Pro or GNA14 p.Gln205Leu demonstrate elongation and black foci. Melanocytes with GNA11 p.Arg183Cys or GNA14 p.Arg179Cys are more spindled and dispersed than those with GNA11 p.Gln209Pro or GNA14 p.Gln205Leu, which exhibit significant piling.

(B) HUVECs with activating mutations in *GNA14* and *GNA11* lose the normal cobblestone morphology seen in wild-type cells and exhibit elongation and disarray.

transduction of primary HUVECs and primary newborn human melanocytes (NBMELs). Given the prevalence of *GNA11* and *GNAQ* mutations in uveal melanoma, we considered melanocytes an important comparator. NBMELs were isolated from human foreskin as previously described,[35] and HUVECs were purchased from the Yale Vascular Biology and Therapeutics Core and maintained in EGM-2 (Lonza). To analyze mutations identified within our cohort and those predicted to be damaging via comparison of amino acid conservation at mutated sites between GNA14 and GNA11, we generated wild-type *GNA14* and *GNA11*, *GNA14* c.614A>T (p.Gln205Leu), *GNA14* c.[535C>T; 537A>T] (p.Arg179Cys), *GNA11* c.626A>C (p.Gln209Pro), and *GNA11* c.547C>T (p.Arg183Cys) via the QuickChange Site-Directed Mutagenesis Kit (Agilent) in the pLVX-Puro lentiviral expression vector (Clontech). Lentiviral particles were packaged in 293T cells with ViraPower Lentiviral Packaging Mix (Thermo Fisher Scientific) according to the manufacturer's instructions and concentrated by centrifugation with the Amicon Ultra-15 Centrifugal Filter Unit with Ultracel-100 (UFC910024, EMD Millipore) prior to adsorption. After 2 days, the growth medium was supplemented with puromycin at 5 μg/ml (NBMELs) or 2 μg/ml (HUVECs) for 72 hr. Afterwards, NBMELs and HUVECs were maintained at a lower puromycin concentration of 1 and 0.5 μg/ml, respectively.

Less than 72 hr after transduction, both HUVECs and NBMELs expressing *GNA14* or *GNA11* mutations demonstrated dramatic changes in morphology in comparison to wild-type controls (Figure 2). NBMELs with GNA11 p.Arg183Cys and GNA14 p.Arg179Cys became elongated, whereas those with GNA11 p.Gln209Pro and GNA14 p.Gln205Leu grew over each other in piles. Further, large black granules surrounding the nucleus were noted in all mutant NBMELs (Figure 2). Electron microscopy with a FEI Tecnai transmission electron microscope at 80 kV accelerating voltage revealed these foci to be large vacuolar structures resembling autophagosomes containing degraded melanin or melanosomes; indeed, cell pellets of NBMELs with *GNA14* and *GNA11* mutations were lighter in color than those of wild-type and untransduced parental controls (Figure S5).[36] Amounts of tyrosinase and Pmel17, markers of melanogenesis and intact melanosomes, respectively, were also found to be reduced in response to the mutations (Figure S5).[37,38] NBMELs transduced with *KRAS* c.35G>A (p.Gly12Asp) and *BRAF* c.1799T>A (p.Val600Glu) did not exhibit these black foci (Figure S6). HUVECs with GNA14 p.Arg179Cys and p.Gln205Leu and GNA11 p.Arg183Cys and p.Gln209Pro also lost organized cobblestone morphology characteristic of normal HUVECs and became markedly elongated, whereas cells transduced with wild-type constructs and vector controls showed normal morphology (Figure 2). HUVECs with KRAS p.Gly12Asp and both wild-type and p.Val600Glu BRAF were elongated and dysplastic (Figure S6).

Given the morphologic changes in cells expressing *GNA14* and *GNA11* mutations, we considered the possibility that the cells were developing features of oncogenic transformation, one in vitro hallmark of which is prolonged survival and proliferation in the absence of

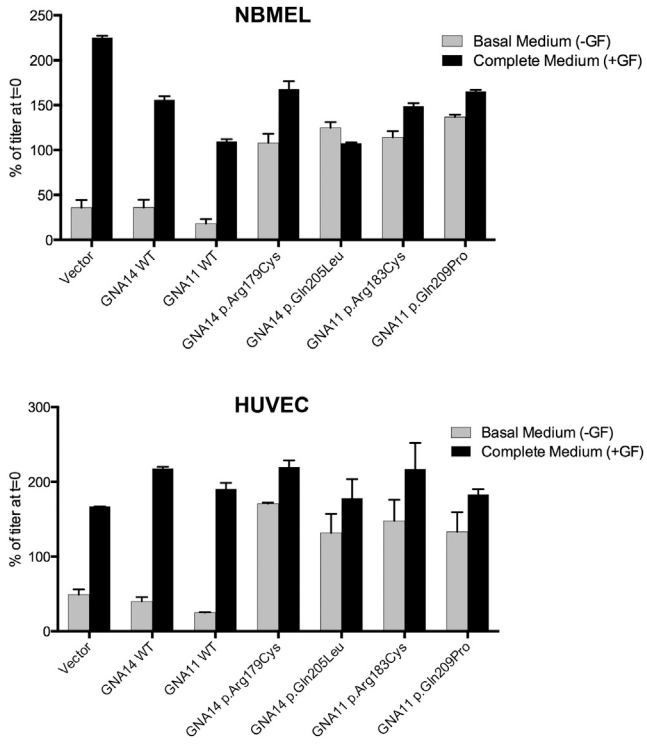

Figure 3. Activating Mutations in *GNA14* and *GNA11* Render NBMELs and HUVECs Growth-Factor Independent
Mutant NBMELs (top) and HUVECs (bottom) are able to survive in basal medium depleted of growth factors.

growth factors.[39–41] Transduced NBMELs and HUVECs were cultured in either basal medium without growth factors required for their proliferation (NBMELs: IBMX, dbcCAMP, and bFGF; HUVECs: EGM-2 Bullets) or complete medium and were assessed for cell viability after 48 hr with the CellTiter-Glo Luminescent Cell Viability Assay (Promega). NBMELs and HUVECs expressing wild-type *GNA14* and *GNA11* and parental cells ceased growth or died in medium without growth factors, whereas NBMELs and HUVECs with GNA14 p.Arg179Cys and p.Gln205Leu and GNA11 p.Arg183Cys and p.Gln209Pro were successfully maintained and passaged in both conditions, suggesting the acquisition of growth-factor independence (Figure 3).

Assessment of the activity of the MAPK pathway showed significant upregulation of activated ERK1/2 in HUVECs and NBMELs expressing mutant but not wild-type *GNA14* or *GNA11* and no evidence of AKT activation (Figure 4). In contrast, KRAS p.Gly12Asp showed increased amounts of p-AKT (Figure 4). These findings suggest that the *GNA14* and *GNA11* mutations we found in KHEs, TAs, and LCHs induce changes in cellular morphology and growth-factor independence via MAPK activation.

To date, mutations in *GNA14* have not been associated with disease, although increased amounts of GNA14 were observed within pulmonary artery endothelial and smooth muscle cells in subjects with pulmonary arterial hypertension, as well as within the endothelial cells of human placentas from pre-eclamptic pregnancies.[42,43] A multiple-candidate-gene approach for surveying hypertension susceptibility genes among a cohort of 3,305 hypertensive and 3,827 normotensive control subjects identified a significant positive association between *GNA14* and *RGS20* (regulator of G-protein signaling 20 [MIM: 607193]) and hypertension, further implicating *GNA14* in vascular biology.[44] Recently, consistent with our findings, constitutive activation of GNA14 was shown to increase RAS activation and downstream phosphorylation of ERK.[45]

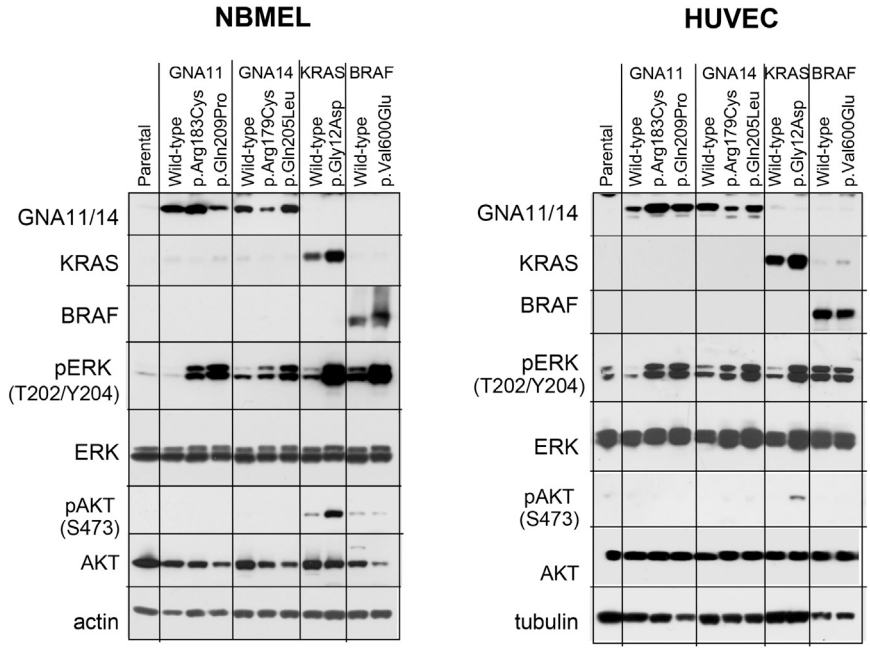

Figure 4. *GNA14* and *GNA11* Mutations Upregulate the MAPK Pathway in NBMELs and HUVECs Independently of AKT Activation
Activating mutations in *GNA14* and *GNA11* upregulate phosphorylation of ERK1/2 in NBMELs (left) and HUVECs (right). GNA14 p.Arg179Cys and GNA11 p.Arg183Cys induce lower p-ERK levels in both cell types than do GNA14 p.Gln205Leu and GNA11 p.Gln209Pro. The membranes were probed with antibodies against GNA11 (D-17, Santa Cruz), GNA14 (SAB4300771, Sigma-Aldrich), BRAF (AF3424, R&D), KRAS (3B10-2F2 WH0003845M1, Sigma-Aldrich), pERK p44/42K T202/Y204 (E10, 9106, Cell Signaling Technology), ERK (4695, Cell Signaling Technology), phospho AKT S473 (9271, Cell Signaling Technology), AKT (9272, Cell Signaling Technology), and β-actin (A1978, Sigma-Aldrich) or tubulin (T5168 Sigma-Aldrich) as controls for protein loading.

Vascular phenotypes resulting from mutations affecting $G_{\alpha q}$ family members range from vascular stains, such as PWSs and capillary malformations, to frank tumors. Our identification of *GNA14* mutations in KHEs, TAs, and LCHs—three distinct classes of vascular tumors—also highlights the pleiotropy of $G_{\alpha q}$ variants, as seen in *GNAQ* and *GNA11* mutations causing LCHs, PWSs, and NICHs.[10–12,16,19] Similarly, activating mutations in *HRAS*, *KRAS*, and *NRAS* also demonstrate phenotypic heterogeneity within vascular anomalies, giving rise to both LCHs and NICHs.[8,9] It remains unclear how identical somatic mutations can give rise to distinct clinical phenotypes. Although *GNA15* and *GNA16* mutations have not yet been identified, they could, in theory, contribute to vascular pathology.

In summary, we have identified a recurrent somatic activating *GNA14* mutation in two congenital vascular tumors and one LCH and found *GNA11* c.547C>T (p.Arg183Cys) in two LCHs. We have shown that mutations in *GNA14* and *GNA11* induce changes in cellular morphology and render cells growth-factor independent via MAPK activation. These findings and recent discoveries that activating mutations in *HRAS*, *KRAS*, *NRAS*, and *BRAF* also drive vascular tumors raise the possibility that inhibition of the MAPK pathway could be an effective therapeutic approach in congenital hemangiomas and infantile vascular lesions unresponsive to conventional therapy.

Accession Numbers

The accession number for the sequencing data reported in this paper is dbGAP: phs000744.

Supplemental Data

Supplemental Data include six figures and two tables and can be found with this article online at http://dx.doi.org/10.1016/j.ajhg.2016.06.010.

Acknowledgments

We thank Xinran Liu for assistance with electron-microscopy images, Elaine Zhou, Jing Zhou, Rong-Hua Hu, and Jonathan Levinsohn for technical assistance, Jordan Pober and William Chang for insightful correspondence on vascular biology, and members of the Yale Center Mendelian Genomics, including Richard P. Lifton, Shrikant M. Mane, and Kaya Bilguvar. This study was supported by a Doris Duke Charitable Foundation Clinical Scientist Development Award to K.A.C. and by the Yale Center for Mendelian Genomics (NIH U54 HG006504). Y.H.L. was supported by the Medical Scientist Training Program at Yale University (NIH/NIGMS T32 GM007205) and is a recipient of the Clinical Mentorship Award from the Doris Duke Charitable Foundation. R.H., A.B., and R.S. are supported by Yale SPORE in Skin Cancer, funded by the NIH National Cancer Institute under award number 1 P50 CA121974 (R.H.).

Received: May 23, 2016
Accepted: June 13, 2016
Published: July 28, 2016

Web Resources

1000 Genomes, http://www.1000genomes.org
COSMIC, http://cancer.sanger.ac.uk/cancergenome/projects/cosmic/
dbGaP, http://www.ncbi.nlm.nih.gov/gap
ExAC Browser, http://exac.broadinstitute.org/
IGV, http://www.broadinstitute.org/igv/
NHLBI Exome Sequencing Project (ESP) Exome Variant Server, http://evs.gs.washington.edu/EVS/
OMIM, http://www.omim.org/
RefSeq, http://www.ncbi.nlm.nih.gov/RefSeq
UCSC Genome Browser, http://genome.ucsc.edu

References

1. North, P.E., Waner, M., Buckmiller, L., James, C.A., and Mihm, M.C., Jr. (2006). Vascular tumors of infancy and childhood: beyond capillary hemangioma. Cardiovasc. Pathol. *15*, 303–317.
2. North, P.E., Waner, M., Mizeracki, A., and Mihm, M.C., Jr. (2000). GLUT1: a newly discovered immunohistochemical marker for juvenile hemangiomas. Hum. Pathol. *31*, 11–22.
3. O'Rafferty, C., O'Regan, G.M., Irvine, A.D., and Smith, O.P. (2015). Recent advances in the pathobiology and management of Kasabach-Merritt phenomenon. Br. J. Haematol. *171*, 38–51.
4. Chiu, Y.E., Drolet, B.A., Blei, F., Carcao, M., Fangusaro, J., Kelly, M.E., Krol, A., Lofgren, S., Mancini, A.J., Metry, D.W., et al. (2012). Variable response to propranolol treatment of kaposiform hemangioendothelioma, tufted angioma, and Kasabach-Merritt phenomenon. Pediatr. Blood Cancer *59*, 934–938.
5. Drolet, B.A., Frommelt, P.C., Chamlin, S.L., Haggstrom, A., Bauman, N.M., Chiu, Y.E., Chun, R.H., Garzon, M.C., Holland, K.E., Liberman, L., et al. (2013). Initiation and use of propranolol for infantile hemangioma: report of a consensus conference. Pediatrics *131*, 128–140.
6. Jain, V., Roychoudhury, S., Chadha, R., and Puri, A. (2012). Variable response to propranolol therapy for infantile hemangiomas. Indian J. Dermatol. *57*, 126–127.
7. Mulliken, J.B., and Enjolras, O. (2004). Congenital hemangiomas and infantile hemangioma: missing links. J. Am. Acad. Dermatol. *50*, 875–882.
8. Groesser, L., Peterhof, E., Evert, M., Landthaler, M., Berneburg, M., and Hafner, C. (2015). BRAF and RAS Mutations in Sporadic and Secondary Pyogenic Granuloma. J. Invest. Dermatol. Published online September 29, 2015. http://dx.doi.org/10.1038/jid.2015.376.
9. Lim, Y.H., Douglas, S.R., Ko, C.J., Antaya, R.J., McNiff, J.M., Zhou, J., Choate, K.A., and Narayan, D. (2015). Somatic Activating RAS Mutations Cause Vascular Tumors Including Pyogenic Granuloma. J. Invest. Dermatol. *135*, 1698–1700.
10. Ayturk, U.M., Couto, J.A., Hann, S., Mulliken, J.B., Williams, K.L., Huang, A.Y., Fishman, S.J., Boyd, T.K., Kozakewich, H.P., Bischoff, J., et al. (2016). Somatic Activating Mutations in GNAQ and GNA11 Are Associated with Congenital Hemangioma. Am. J. Hum. Genet. *98*, 789–795.
11. Funk, T., Lim, Y.H., Kulungowski, A.M., Prok, L., Crombleholme, T.M., Choate, K.A., and Bruckner, A.L. Symptomatic Congenital Hemangioma and Congenital "Hemangiomatosis" Associated with a Somatic Activating Mutation in GNA11. J. Am. Med. Assoc. Dermatology. Published online

July 20, 2016. http://dx.doi.org/10.01/jamadermatol.2016.2365.
12. Nakashima, M., Miyajima, M., Sugano, H., Iimura, Y., Kato, M., Tsurusaki, Y., Miyake, N., Saitsu, H., Arai, H., and Matsumoto, N. (2014). The somatic GNAQ mutation c.548G>A (p.R183Q) is consistently found in Sturge-Weber syndrome. J. Hum. Genet. *59*, 691–693.
13. Shirley, M.D., Tang, H., Gallione, C.J., Baugher, J.D., Frelin, L.P., Cohen, B., North, P.E., Marchuk, D.A., Comi, A.M., and Pevsner, J. (2013). Sturge-Weber syndrome and port-wine stains caused by somatic mutation in GNAQ. N. Engl. J. Med. *368*, 1971–1979.
14. Zeng, H., Zhao, D., Yang, S., Datta, K., and Mukhopadhyay, D. (2003). Heterotrimeric G alpha q/G alpha 11 proteins function upstream of vascular endothelial growth factor (VEGF) receptor-2 (KDR) phosphorylation in vascular permeability factor/VEGF signaling. J. Biol. Chem. *278*, 20738–20745.
15. Sivaraj, K.K., Li, R., Albarran-Juarez, J., Wang, S., Tischner, D., Grimm, M., Swiercz, J.M., Offermanns, S., and Wettschureck, N. (2015). Endothelial Gαq/11 is required for VEGF-induced vascular permeability and angiogenesis. Cardiovasc. Res. *108*, 171–180.
16. Thomas, A.C., Zeng, Z., Rivière, J.B., O'Shaughnessy, R., Al-Olabi, L., St-Onge, J., Atherton, D.J., Aubert, H., Bagazgoitia, L., Barbarot, S., et al. (2016). Mosaic Activating Mutations in GNA11 and GNAQ Are Associated with Phakomatosis Pigmentovascularis and Extensive Dermal Melanocytosis. J. Invest. Dermatol. *136*, 770–778.
17. Van Raamsdonk, C.D., Griewank, K.G., Crosby, M.B., Garrido, M.C., Vemula, S., Wiesner, T., Obenauf, A.C., Wackernagel, W., Green, G., Bouvier, N., et al. (2010). Mutations in GNA11 in uveal melanoma. N. Engl. J. Med. *363*, 2191–2199.
18. Chu, C.Y., Hsiao, C.H., and Chiu, H.C. (2003). Transformation between Kaposiform hemangioendothelioma and tufted angioma. Dermatology (Basel) *206*, 334–337.
19. Couto, J.A., Huang, L., Vivero, M.P., Kamitaki, N., Maclellan, R.A., Mulliken, J.B., Bischoff, J., Warman, M.L., and Greene, A.K. (2016). Endothelial Cells from Capillary Malformations Are Enriched for Somatic GNAQ Mutations. Plast. Reconstr. Surg. *137*, 77e–82e.
20. Li, H., and Durbin, R. (2009). Fast and accurate short read alignment with Burrows-Wheeler transform. Bioinformatics *25*, 1754–1760.
21. Van der Auwera, G.A., Carneiro, M.O., Hartl, C., Poplin, R., Del Angel, G., Levy-Moonshine, A., Jordan, T., Shakir, K., Roazen, D., Thibault, J., et al. (2013). From FastQ data to high confidence variant calls: the Genome Analysis Toolkit best practices pipeline. Curr. Protoc. Bioinformatics *43*, 11.10.1–11.10.33.
22. Wang, K., Li, M., and Hakonarson, H. (2010). ANNOVAR: functional annotation of genetic variants from high-throughput sequencing data. Nucleic Acids Res. *38*, e164.
23. Cibulskis, K., Lawrence, M.S., Carter, S.L., Sivachenko, A., Jaffe, D., Sougnez, C., Gabriel, S., Meyerson, M., Lander, E.S., and Getz, G. (2013). Sensitive detection of somatic point mutations in impure and heterogeneous cancer samples. Nat. Biotechnol. *31*, 213–219.
24. Thorvaldsdóttir, H., Robinson, J.T., and Mesirov, J.P. (2013). Integrative Genomics Viewer (IGV): high-performance genomics data visualization and exploration. Brief. Bioinform. *14*, 178–192.
25. Malhotra, Y., Yang, C.S., McNamara, J., and Antaya, R.J. (2014). Congenital kaposiform hemangioendothelioma with Kasabach-Merritt phenomenon successfully treated with low-dose radiation therapy. Pediatr. Dermatol. *31*, 595–598.
26. Hubbard, K.B., and Hepler, J.R. (2006). Cell signalling diversity of the Gqalpha family of heterotrimeric G proteins. Cell. Signal. *18*, 135–150.
27. Wettschureck, N., and Offermanns, S. (2005). Mammalian G proteins and their cell type specific functions. Physiol. Rev. *85*, 1159–1204.
28. Heydorn, A., Ward, R.J., Jorgensen, R., Rosenkilde, M.M., Frimurer, T.M., Milligan, G., and Kostenis, E. (2004). Identification of a novel site within G protein alpha subunits important for specificity of receptor-G protein interaction. Mol. Pharmacol. *66*, 250–259.
29. Strathmann, M.P., and Simon, M.I. (1991). G alpha 12 and G alpha 13 subunits define a fourth class of G protein alpha subunits. Proc. Natl. Acad. Sci. USA *88*, 5582–5586.
30. Forbes, S.A., Beare, D., Gunasekaran, P., Leung, K., Bindal, N., Boutselakis, H., Ding, M., Bamford, S., Cole, C., Ward, S., et al. (2015). COSMIC: exploring the world's knowledge of somatic mutations in human cancer. Nucleic Acids Res. *43*, D805–D811.
31. Kelley, L.A., Mezulis, S., Yates, C.M., Wass, M.N., and Sternberg, M.J. (2015). The Phyre2 web portal for protein modeling, prediction and analysis. Nat. Protoc. *10*, 845–858.
32. Pettersen, E.F., Goddard, T.D., Huang, C.C., Couch, G.S., Greenblatt, D.M., Meng, E.C., and Ferrin, T.E. (2004). UCSF Chimera–a visualization system for exploratory research and analysis. J. Comput. Chem. *25*, 1605–1612.
33. Taylor, V.G., Bommarito, P.A., and Tesmer, J.J. (2016). Structure of the Regulator of G Protein Signaling 8 (RGS8)-Gαq Complex: MOLECULAR BASIS FOR Gα SELECTIVITY. J. Biol. Chem. *291*, 5138–5145.
34. Kimple, A.J., Bosch, D.E., Giguère, P.M., and Siderovski, D.P. (2011). Regulators of G-protein signaling and their Gα substrates: promises and challenges in their use as drug discovery targets. Pharmacol. Rev. *63*, 728–749.
35. Krauthammer, M., Kong, Y., Ha, B.H., Evans, P., Bacchiocchi, A., McCusker, J.P., Cheng, E., Davis, M.J., Goh, G., Choi, M., et al. (2012). Exome sequencing identifies recurrent somatic RAC1 mutations in melanoma. Nat. Genet. *44*, 1006–1014.
36. Drochmans, P. (1960). Electron microscope studies of epidermal melanocytes, and the fine structure of melanin granules. J. Biophys. Biochem. Cytol. *8*, 165–180.
37. Leonhardt, R.M., Vigneron, N., Hee, J.S., Graham, M., and Cresswell, P. (2013). Critical residues in the PMEL/Pmel17 N-terminus direct the hierarchical assembly of melanosomal fibrils. Mol. Biol. Cell *24*, 964–981.
38. Chang, T.S. (2009). An updated review of tyrosinase inhibitors. Int. J. Mol. Sci. *10*, 2440–2475.
39. Boswell, H.S., Nahreini, T.S., Burgess, G.S., Srivastava, A., Gabig, T.G., Inhorn, L., Srour, E.F., and Harrington, M.A. (1990). A RAS oncogene imparts growth factor independence to myeloid cells that abnormally regulate protein kinase C: a nonautocrine transformation pathway. Exp. Hematol. *18*, 452–460.
40. Rodeck, U. (1993). Growth factor independence and growth regulatory pathways in human melanoma development. Cancer Metastasis Rev. *12*, 219–226.
41. Wang, L., and Damania, B. (2008). Kaposi's sarcoma-associated herpesvirus confers a survival advantage to endothelial cells. Cancer Res. *68*, 4640–4648.
42. Lei, W., Chen, P., Yue, Y., He, Y., Shui, X., Li, G., Zhang, L., Huang, S., and Chen, C. (2014). Subcellular distribution patterns and elevated expression of GNA11 and GNA14 proteins

in the lungs of humans with pulmonary arterial hypertension. Cell Biol. Int. *38*, 1041–1049.

43. Zhao, Y.J., Zou, Q.Y., Li, Y., Li, H.H., Wu, Y.M., Li, X.F., Wang, K., and Zheng, J. (2014). Expression of G-protein subunit α-14 is increased in human placentas from preeclamptic pregnancies. J. Histochem. Cytochem. *62*, 347–354.
44. Kohara, K., Tabara, Y., Nakura, J., Imai, Y., Ohkubo, T., Hata, A., Soma, M., Nakayama, T., Umemura, S., Hirawa, N., et al. (2008). Identification of hypertension-susceptibility genes and pathways by a systemic multiple candidate gene approach: the millennium genome project for hypertension. Hypertens. Res. *31*, 203–212.
45. Kwan, D.H., Yung, L.Y., Ye, R.D., and Wong, Y.H. (2012). Activation of Ras-dependent signaling pathways by G(14) -coupled receptors requires the adaptor protein TPR1. J. Cell. Biochem. *113*, 3486–3497.

The American Journal of Human Genetics, Volume *99*

Supplemental Data

GNA14 Somatic Mutation Causes Congenital and Sporadic Vascular Tumors by MAPK Activation

Young H. Lim, Antonella Bacchiocchi, Jingyao Qiu, Robert Straub, Anna Bruckner, Lionel Bercovitch, Deepak Narayan, Yale Center for Mendelian Genomics, Jennifer McNiff, Christine Ko, Leslie Robinson-Bostom, Richard Antaya, Ruth Halaban, and Keith A. Choate

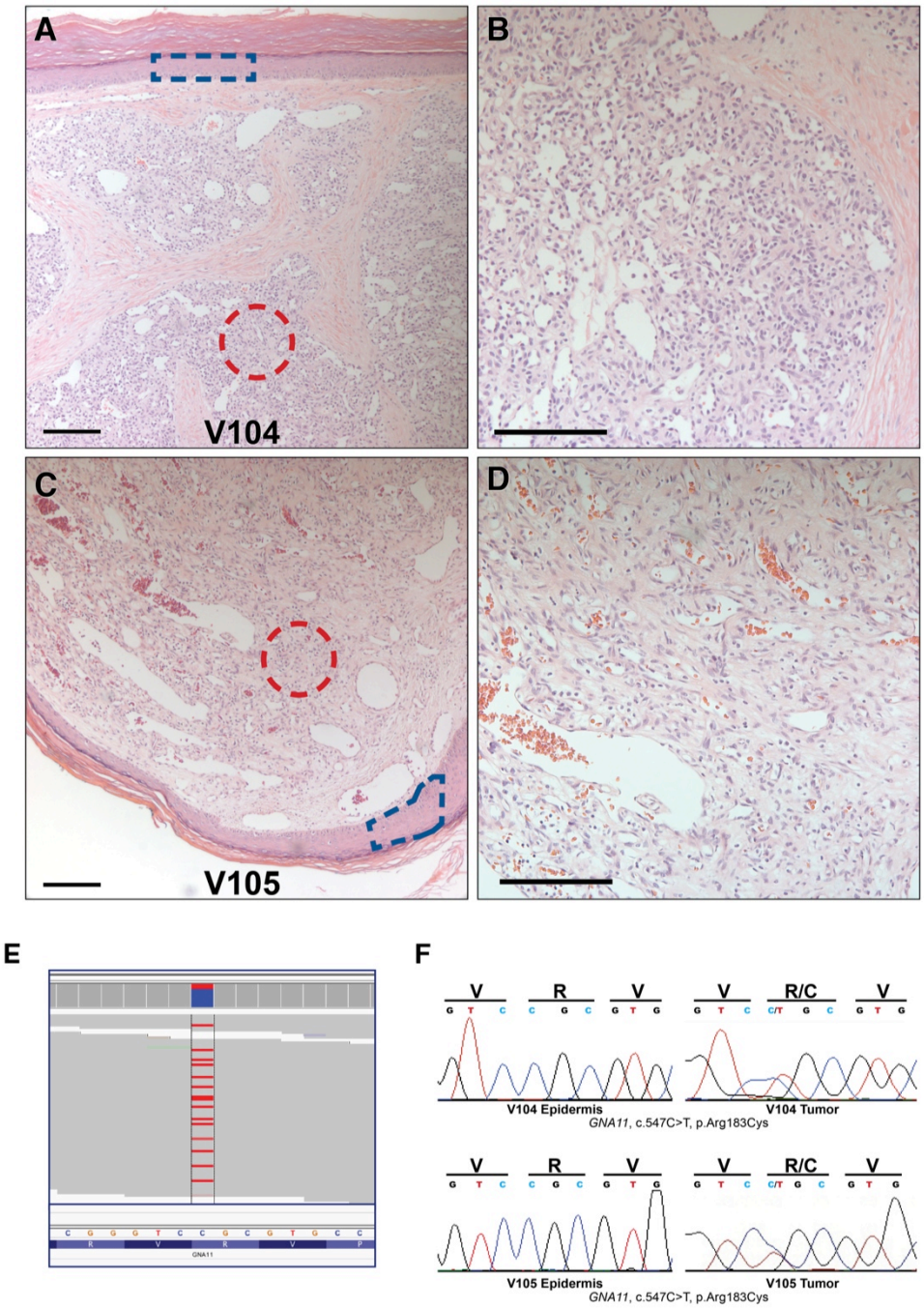

Figure S1. Somatic *GNA11* c.547C>T (p.Arg183Cys) mutation causes sporadic lobular capillary hemangiomas. (A-D) V104 and V105 are sporadic lobular capillary hemangiomas with histology at **(A,C)** 10X and **(B,D)** 20X magnification showing classic keratinized encapsulation of proliferating lobular capillaries. Areas where LCM was employed to isolate tissue for DNA is shown for unaffected epidermis (blue boxes), and tumor (red circles). **(E)** IGV of V104 exome data demonstrates 16/71 (22%) non-reference reads corresponding to c.547C>T (p.Arg183Cys). **(F)** Sanger sequencing of unaffected epidermis and tumor of V104 and V105 shows *GNA11* c.547C>T (p.Arg183Cys) in tumor only. Scale bars = 150μm.

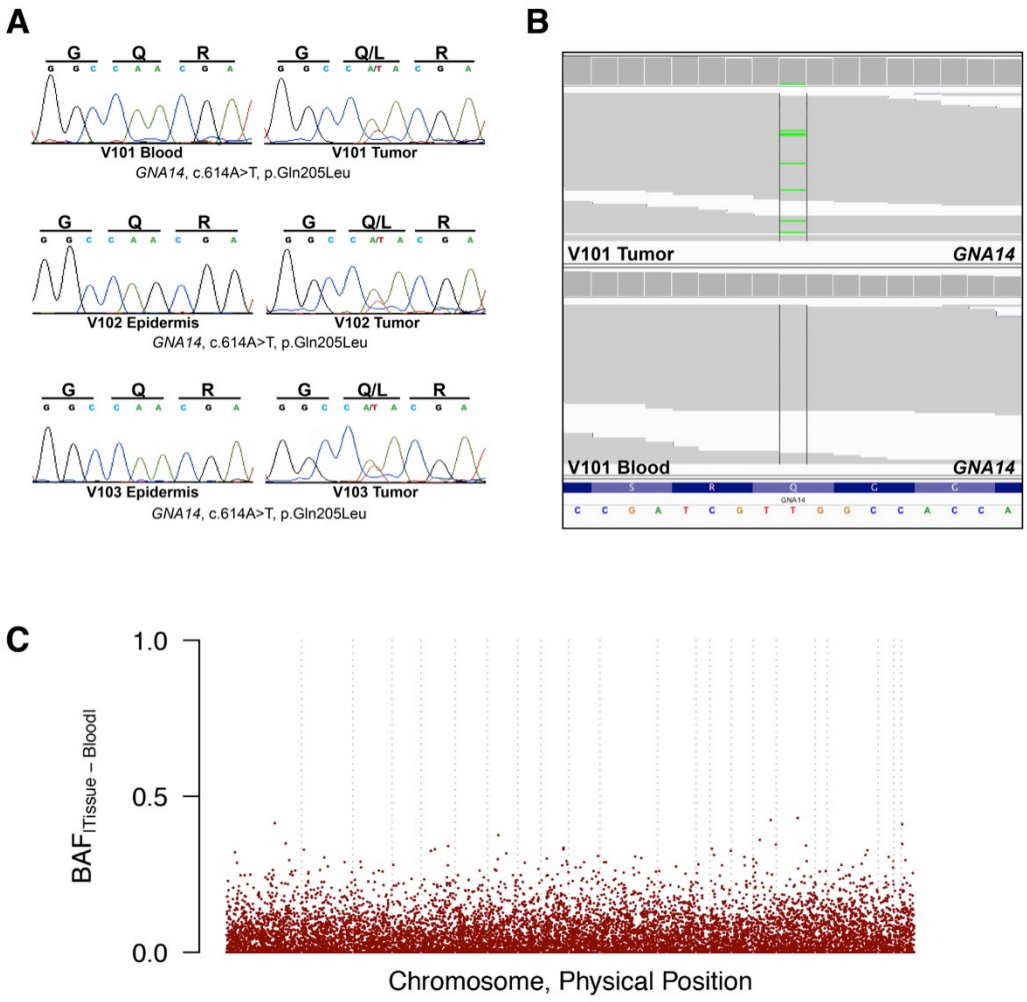

Figure S2. *GNA14* c.614A>T (p.Gln205Leu) mutation in vascular tumors. (A) Sanger sequencing traces show somatic *GNA14* c.614A>T (p.Gln205Leu) mutation in all 3 samples. **(B)** Integrated genome viewer (IGV) plots of exome sequencing data from V101 show 7/78 (9%) and 0/96 non-reference reads in tumor and blood, respectively. **(C)** Plot of B-allele frequency (BAF) demonstrates no segments of loss-of-heterozygosity or copy number variation in V101. Dotted lines separate individual chromosomes.

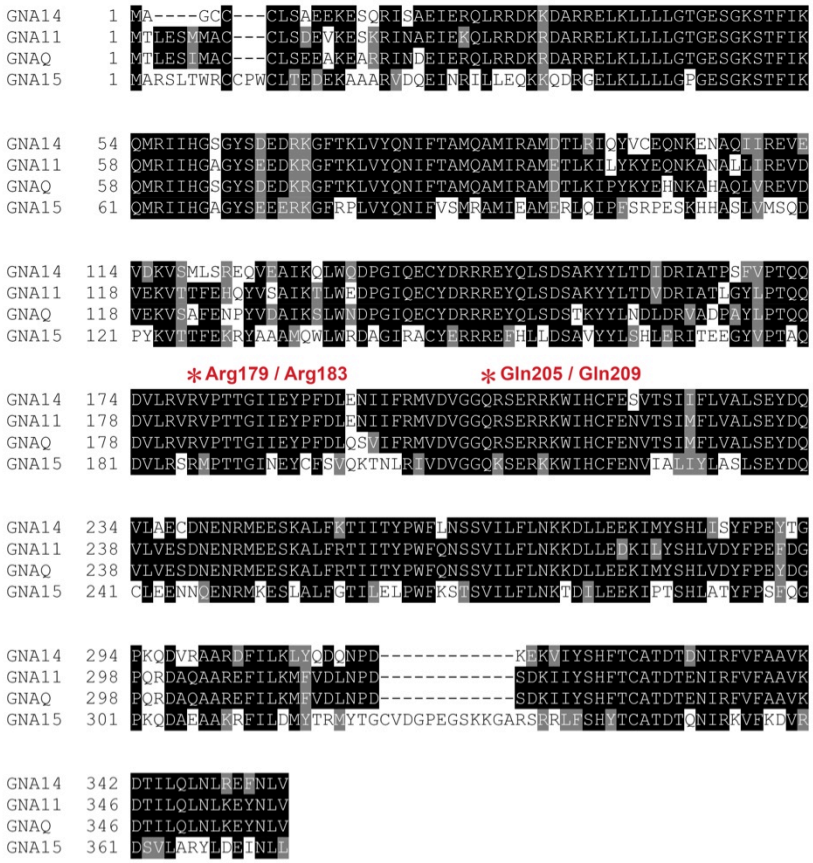

Figure S3. Sequence homology among members of the Gαq family. Arginine at positions 179 (GNA14) and 183 (GNA11) and glutamine at positions 205 (GNA14) and 209 (GNA11) (red asterisks) are conserved among all Gαq members.

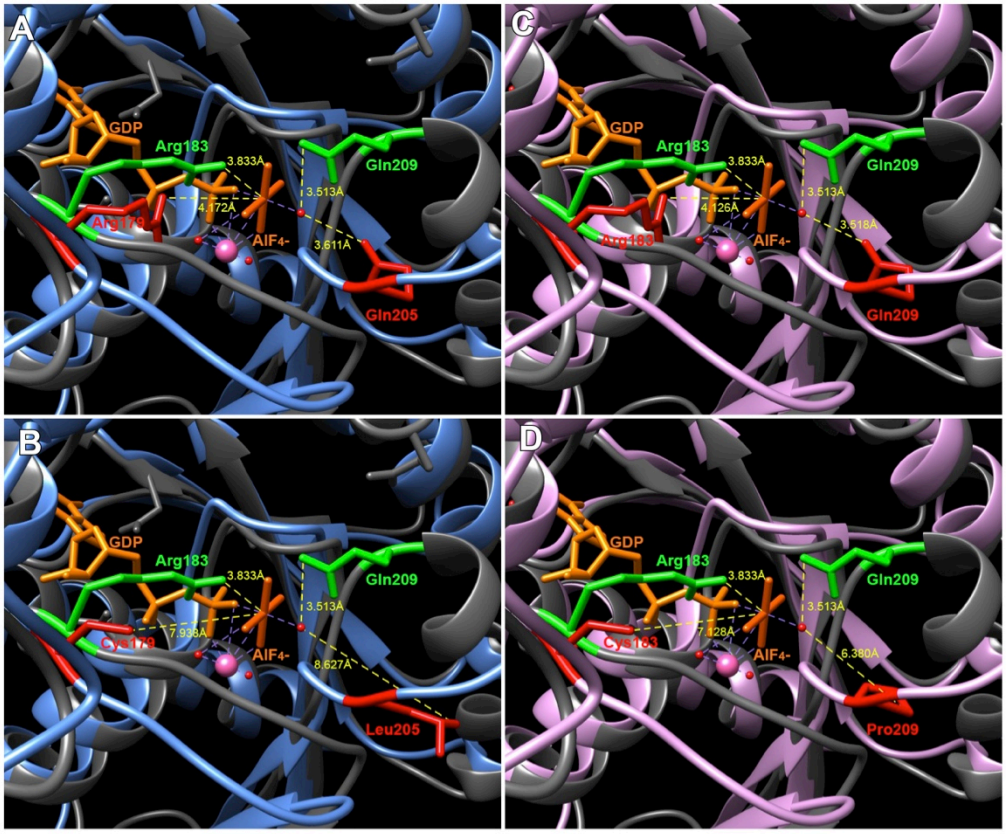

Figure S4. *GNA14* and *GNA11* mutations disrupt stabilization within the GTPase catalytic core. Phyre2 was employed to construct a theoretical model of GNA14 (A,B, blue) and GNA11 (C, D, pink) GTPase domains, which were overlaid with an established GNAQ template (A-D, grey). Residues in which mutation causes vascular tumors are highlighted in red (GNA14 and GNA11), and green (GNAQ). Molecular distance from stabilized moieties are labeled (yellow dashed lines). The transition state of bound GDP-AlF_4^- (orange)—representing GTP—undergoing hydrolysis is stabilized (purple dashed lines) by Mg^{2+} (pink sphere) and water moieties (red spheres) in the catalytic core. **(A)** Native GNA14 showing arginine 179 and glutamine 205, with corresponding GNAQ arginine 183 and glutamine 209. GNA14 arginine 179, like GNAQ arginine 183, stabilizes the leaving γ-phosphate, and in its native state, is 4.172Å from AlF_4^-. GNA14 glutamine 205, like GNAQ glutamine 209, stabilizes the water moiety driving hydrolysis of the γ-phosphate, and is 3.611Å away. **(B)** GNA14 with both p.Arg179Cys and p.Gln205Leu protein changes, with corresponding native GNAQ residues. Cysteine 179 and leucine 205 are distanced further from the γ-phosphate at 7.938Å and 8.627Å, respectively, and lose their stabilizing amide groups. **(C)** Native GNA11 with arginine 183 and glutamine 209, and corresponding residues in GNAQ. GNA11 arginine 183 is 4.126Å from AlF_4^-, while GNA11 glutamine 209 is 3.518Å from the nucleophilic water molecule. **(D)** GNA11 with p.Arg183Cys and p.Gln209Pro and corresponding native GNAQ residues shows GNA11 mutant residues are further away, with cysteine 183 at 7.128Å, and proline 209 at 6.380Å.

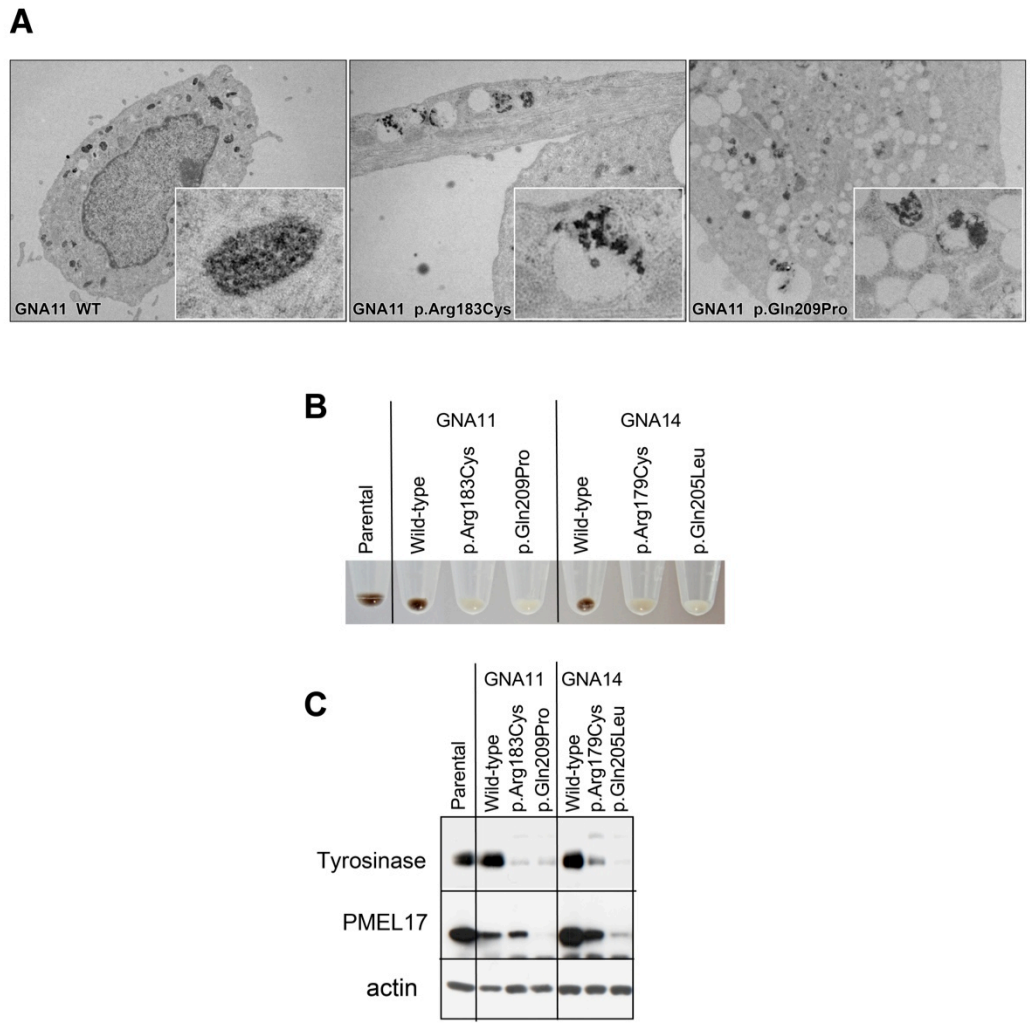

Figure S5. Activating *GNA11* and *GNA14* mutations result in loss of pigment in NBMELs. (A) Electron microscopy of NBMELs (GNA11 wild type, p.Arg183Cys, and p.Gln209Pro shown as representative) demonstrates melanosome degradation within vacuolar structures in the mutants, resulting in loss of cellular pigment (**B)**. **(C)** *GNA11* and *GNA14* mutations lead to lower levels of tyrosinase and Pmel17, markers of melanogenesis and intact melanosomes, respectively. The membrane was probed with antibodies against tyrosinase (T311, NeoMarker) and Pmel17,[1] and β-Actin (A1978, Sigma-Aldrich) as control for protein loading.

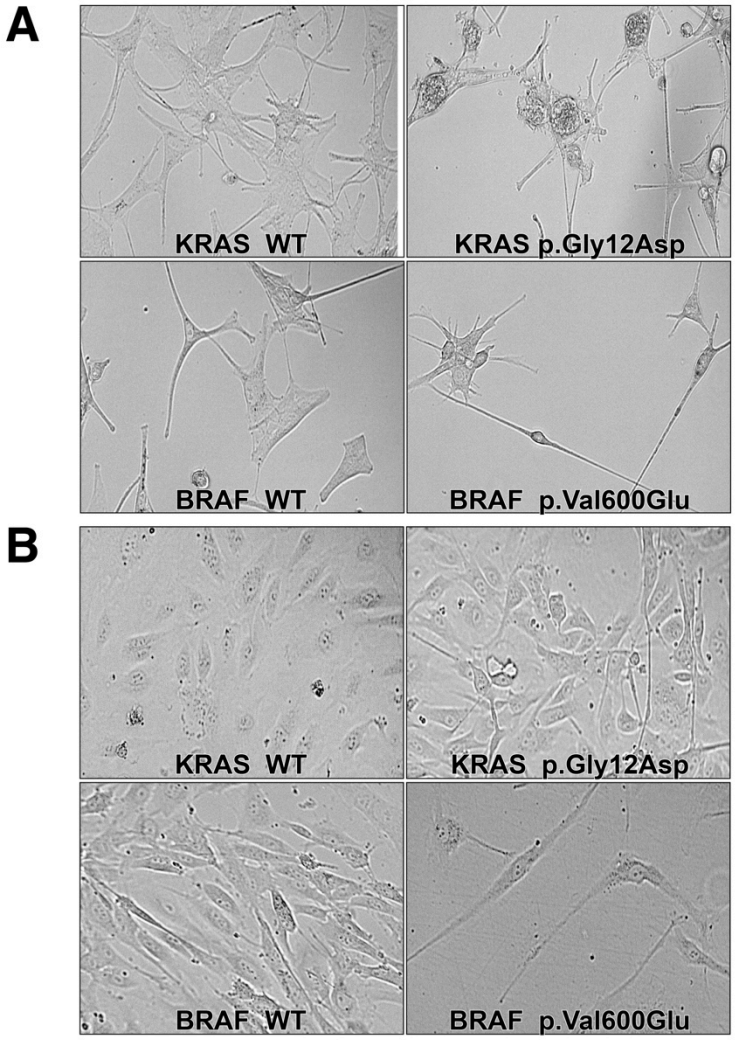

Figure S6. Activating *KRAS* and *BRAF* mutation in NBMEL and HUVEC lead to changes in morphology. (A) NBMELs expressing *KRAS* wild type and c.35G>A (p.Gly12Asp) and *BRAF* wild type and c.1799T>A (p.Val600Glu) mutation. (**B)** HUVECs expressing *KRAS* and *BRAF* wild type and mutation.

Sample	Mean Coverage	Bases Covered >8x	Bases Covered >20x	Mean Read Length
V101 Tissue	94x	97%	92%	74 bases
V101 Blood	89x	98%	91%	74 bases
V104 Tissue	68x	97%	88%	74 bases

Table S1. Exome coverage statistics. In all samples, >97% of coding regions are covered >8x, sufficient for analysis. 74bp paired-end sequencing of tissue and blood from V101 and tissue from V104 was performed by shearing and barcoding genomic DNA, followed by capture using Roche EZ Exome V3 capture probes. Sequencing was performed on the Illumina HiSeq 2500, with tissue samples run at 4 per lane, and blood run at 6 per lane. Sequence was aligned to the hg19 reference using BWA-MEM, trimmed, and PCR duplicates removed using Picard. BAM files were calibrated using GATK.

Filter	V101
All SSNVs	37
In exons/splice Site	20
Nonsynonymous	10
<0.1% Prevalence in ExAC	1 (*GNA14*)
Fisher's Test p-value < 1.0×10^{-2}	1 (*GNA14*)

Table S2. Somatic single nucleotide variant (SSNV) filtering. Somatic mutations were identified by employing a Perl script alongside MuTect. Called SSNVs were filtered to exclude intronic and intergenic variants, synonymous mutations, and mutations listed in ExAC, 1000 Genomes, the NHLBI Exome Variant Server, and dbSNP control datasets. The remaining variants were visualized using Integrative Genome Viewer (IGV) to inspect for mismapped reads. The single remaining *GNA14* mutation was validated with Sanger sequencing, and confirmed via laser capture microdissection in V102 and V103 (Figure S2).

SUPPLEMENTAL REFERENCES

1. Lee, Z.H., Hou, L., Moellmann, G., Kuklinska, E., Antol, K., Fraser, M., Halaban, R., and Kwon, B.S. (1996). Characterization and subcellular localization of human Pmel 17/silver, a 110-kDa (pre)melanosomal membrane protein associated with 5,6,-dihydroxyindole-2-carboxylic acid (DHICA) converting activity. The Journal of investigative dermatology 106, 605-610.